Available online at www.sciencedirect.com
ScienceDirect
Geochimica et Cosmochimica Acta 72 (2008) 140–150
Geochimica et Cosmochimica Acta
www.elsevier.com/locate/gca

Characterizing solution and solid-phase amorphous uranyl silicates ☆

L. Soderholm [a,*], S. Skanthakumar [a], D. Gorman-Lewis [a], M.P. Jensen [a], K.L. Nagy [b]

[a] Chemistry Division, Argonne National Laboratory, CHM/200, 9700 S. Cass Avenue, Argonne, IL 60439, USA
[b] Department of Earth and Environmental Sciences, MC-186, 845 West Taylor Street, University of Illinois at Chicago, Chicago, IL 60607, USA

Received 8 June 2007; accepted in revised form 2 October 2007; available online 12 October 2007

Abstract

A combination of high-energy X-ray scattering (HEXS) and X-ray diffraction (XRD) is used to structurally and chemically characterize uranyl-silicate solutions and precipitates. Starting with a U to Si ratio of 1:2, solutions prepared at room temperature from pH 2.2 to 9.0 and at 150 °C from pH 5.1 to 9.1 showed U–U correlations out to distances of 10 Å or longer in both final solutions and precipitates. With one exception, all of the precipitates were amorphous, with no evidence of Bragg diffraction in the XRD data. The room temperature samples above pH 3.1 all had similar Fourier transforms of their HEXS data, which were obtained from suspended slurries or precipitates. In contrast, the hydrothermal sample precipitates showed considerable variation in their HEXS correlations at longer distances. The XRD pattern of the hydrothermal sample with a pH of 5.1 exhibited Bragg reflections indexable as soddyite. While showing no evidence of crystallinity using XRD, the hydrothermal sample at pH 6 showed similar HEXS correlations, which evolved in samples at increasing pH into correlations more consistent with sodium boltwoodite. These findings are supported by thermodynamic modeling. The structural correlations seen in the HEXS data to distances of about 4 Å are similar in all samples prepared at pH 4 or higher. This similarity of structure is used to propose a model for solid formation that includes a uranyl silicate building block, or synthon, which preorganizes in solution. Varying the pH changes how these synthons link into larger structures.

1. INTRODUCTION

Dissolved uranium, as the uranyl ion UO_2^{2+}, is considered a contaminant introduced into the environment near mining, processing and production operations worldwide. A predictive understanding of its mobility, transport, and fate under geologically relevant conditions is severely hampered by its chemistry in near neutral or basic groundwater, where it can undergo hydrolysis, complexation, and oligomerization reactions. Available mineral surfaces and dissolved anions, in combination with groundwater Eh and pH are known to play a central role in uranyl-ion transport. A well studied example is the interaction of uranyl with dissolved silica (Porter and Weber, 1971; Satoh and Choppin, 1992; Jensen and Choppin, 1998; Moll et al., 1998; Hrnecek and Irlweck, 1999; Yusov and Fedoseev, 2005), silica gels (Reich et al., 1998; Allard et al., 1999; Gabriel et al., 2001) and silicate-mineral surfaces (Chisholm-Brause et al., 1994; Hudson et al., 1999; Waite et al., 2000; Froideval et al., 2003; Walter et al., 2005; Arai et al., 2006). Although the mineral geochemistry of uranyl silicates

☆ The submitted manuscript has been created by University of Chicago, Argonne, LLC, Operator of Argonne National Laboratory ("Argonne"). Argonne, a U.S. Department of Energy Office of Science laboratory, is operated under Contract No. DE-AC02-06CH11357. The U.S. Government retains for itself, and other acting on its behalf, a paid-up nonexclusive, irrevocable worldwide license in said article to reproduce, prepare derivative works, distribute copies to the public, and perform publicly and display publicly, by or on behalf of the Government.

* Corresponding author. Fax: +1 630 252 4225.
E-mail address: ls@anl.gov (L. Soderholm).

0016-7037/$ - see front matter © 2007 Elsevier Ltd. All rights reserved.
doi:10.1016/j.gca.2007.10.002

(Finch and Murakami, 1999) serves as an important guide, relevant species are often ill-defined amorphous dissolved colloids or precipitates. Understanding the groundwater conditions that favor nucleation, aggregation and/or crystallization of uranyl silicates (Liu et al., 2004; McKinley et al., 2006) is an important aspect of modeling contaminant transport that has not yet been realized.

X-ray diffraction (XRD) is the tool of choice for characterizing solid phases. Whereas this technique has been often applied to uranyl silicates, (ICSD, 2006) it is only effective for samples exhibiting long-range order. Structural and chemical information has been sought for colloidal and amorphous samples through indirect probes such as IR/Raman (Plesko et al., 1992; Frost et al., 2006a,b), NMR (Harris and Newman, 1977; Harris et al., 1980; Cho et al., 2006) optical, (Porter and Weber, 1971; Yusov and Fedoseev, 2005) and fluorescence spectroscopies (Moll et al., 1998; Wang et al., 2005) by comparing spectra to those obtained from known phases. X-ray absorption spectroscopy (XAS), a single-ion probe that provides direct information about structural correlations has been applied liberally to solution and solid-phase samples (Dent et al., 1992; Reich et al., 1996; Giaquinta et al., 1997; Thompson et al., 1997; Hudson et al., 1999; Sylwester et al., 2000; Catalano and Brown, 2004; Catalano et al., 2004; Antonio and Soderholm, 2006). Unfortunately it provides information over a limited distance range, which for the case of uranyl silicates has not proven sufficient to make the necessary structural distinctions between known mineral phases (Thompson et al., 1997; Catalano and Brown, 2004).

Recently, high-energy X-ray scattering (HEXS) has been demonstrated to provide information about atomic correlations in solutions (Neuefeind et al., 2004; Soderholm et al., 2005; Skanthakumar and Soderholm, 2006; Skanthakumar et al., 2007; Wilson et al., 2007) and X-ray amorphous solids (showing no diffraction peaks) to distances of 8–10 Å or longer (Egami and Billinge, 2003). HEXS is particularly well suited to studying dissolved heavy metals because X-rays scatter off electrons and therefore high-Z oligomers have sufficient contrast to be observable in solutions at concentrations down to the millimolar. Lacking the concentration sensitivity, distance resolution, and oxidation state information provided by XAS (Skanthakumar et al., 2007), the ability to extract longer-distance correlations provides an excellent complement to the near-neighbor information currently available from these other techniques.

The Fourier transforms of HEXS spectra provide correlation distances and intensities that can be quantified in terms of the pairs of atomic species involved and the relative concentration of the correlation in solution. Further interpretation of the results, including the assessment of structural entities that are composed of the observed correlations, requires structural and chemical inferences that may be gleaned from the available literature or calculated from appropriate thermodynamic or theoretical modeling.

In this manuscript, we describe XRD and HEXS measurements undertaken to describe the speciation of 0.05 M uranyl in a 1:2 sodium metasilicate solution as a function of pH. The interpretation of observed solution correlations is guided by both structural analogs and thermodynamic calculations that identify potential stable phases. The results are discussed in terms of a preorganized structural unit, or synthon, present in solution and in amorphous precipitates. Variations in structural motifs with pH are then interpreted within the context of building from this unit.

2. EXPERIMENTAL

2.1. Sample preparation

All samples were prepared from stock uranyl perchlorate and sodium metasilicate solutions. The sodium metasilicate solution was prepared by adding sodium metasilicate ($Na_2SiO_3{\cdot}9H_2O$) to 0.17 M perchloric acid to achieve a concentration of 0.105 M. The uranyl perchlorate solution was prepared by adding $UO_3(H_2O)_{0.8}$ to 2.2 M $HClO_4$ and heating gently for ~60 min to achieve a final concentration of 0.990 M U in ca. 2.4 M $HClO_4$. Samples were prepared by adding 50 μL of the stock uranyl perchlorate solution and 950 μL of the stock sodium metasilicate solution to polypropylene centrifuge cones, for final uranyl and silicate concentrations of 50 and 100 mM, respectively. The initial pH of the resulting solution was 3.1. Small amounts of $HClO_4$ or NaOH were added to adjust pH from 2.2 to 9.0 in eight room temperature samples. Four samples from pH 5.1 to 9.1 were prepared using the same procedure as described above and subsequently heated in a Parr bomb for 4 days at 150 °C for the purpose of accelerating the reaction rates.

Stable suspensions were visible immediately in the room temperature samples with pHs greater than about 4. Solids were isolated by centrifugation and the precipitates were washed with deionized water and air-dried at room temperature. The hydrothermally treated samples all resulted in precipitates that were washed and dried in the same manner.

2.2. X-ray diffraction

X-ray powder diffraction data were obtained on the solid phases from the room temperature and the hydrothermal samples using a Scintag theta–theta diffractometer equipped with a Peltier detector and operating with a Cu tube. Approximately 5 mg of powder were placed on a low-background quartz slide with data collected over a 2θ range of 2–120° with a 0.01 step size and a scan rate of 0.1 °/min. The sample holder was measured separately and its diffraction pattern was used for background subtraction.

2.3. High-energy X-ray scattering

The high-energy X-ray scattering data were collected at the Advanced Photon Source, Argonne National Laboratory (wiggler beamline 11-ID-B, BESSRCCAT). The incident beam of 91 keV corresponds to a wavelength of 0.13702 Å, with the scattered intensity measured using a General Electric amorphous silicon flat panel X-ray detector (GE Healthcare) mounted in a static position

($2\theta = 0°$) providing detection in momentum transfer space Q up to 32 $Å^{-1}$ at this fixed geometry. Samples of both solutions and solids were enclosed in Kapton capillaries with epoxy plugs and further contained as required for actinide samples. HEXS data were obtained on the room temperature solutions without removing any suspended solids, on the centrifuged solids from the room temperature experiments, and on the dried solids from the hydrothermal experiments. Data were also obtained on two 100 mM sodium metasilicate solutions at two different pH values (3.9 and 9.0) for background removal from the solution data. The two spectra were indistinguishable so the lower pH solution was used for all background subtractions.

Data were treated as described previously (Skanthakumar and Soderholm, 2006). The X-ray data obtained in these experiments are equivalent to standard powder patterns, that is intensity vs. scattering angle, except that the data are taken out to large momentum transfers (Q). For example, a powder pattern obtained with a copper tube as the X-ray source has a maximum Q of about 8 $Å^{-1}$. This is important because the scattering data are Fourier transformed, to provide a pair-correlation or pair distribution function (PDF), the resolution of which is dependent on the Q range used in the Fourier transform (FT) (Magini et al., 1988; Egami and Billinge, 2003). Peak positions in a PDF represent coordination distances between atoms. The data shown in the figures are obtained by FT of the background subtracted scattering function $S(Q)$, an example of which is shown in Appendix A. The peaks in the $G(r)$ vs. r (Å) plots represent coordination distances of uranium to other atoms and their intensities are related to the relative concentrations of the coordination pairs. For the purposes of this manuscript, only relative peak intensities are considered and $G(r)$ is reported in arbitrary units.

3. RESULTS

3.1. Room temperature samples

The two samples at pH 2.2 and 3.1 appeared clear, whereas the higher pH samples were cloudy, visible evidence of suspensions that did not settle upon sitting for several days. X-ray diffraction patterns of the isolated solids from these samples show a broadly peaked baseline without any well-defined Bragg reflections indicating that all of the samples are X-ray amorphous (Fig. 1a). Furthermore, the locations of the broad peaks are generally consistent with groups of peaks from a variety of crystalline U-phases that might be expected in the experimental system including U-silicates, oxides, hydroxides, and carbonates (Hill, 1999).

Pair distribution functions (PDFs) derived from the background-subtracted HEXS data for the aqueous suspensions prepared at room temperature are shown in Fig. 1b along with a representative PDF for the precipitate, all of which produced indistinguishable spectra. The data obtained for pHs of 5, 6, 6.9, 8, and 9 aqueous suspensions are also indistinguishable, except for slight changes in peak intensities, and are therefore represented in Fig. 1b by the pH 6.9 PDF for the purpose of clarity. Uncertainties in background subtraction resulting from sample inhomogeneities influenced the lower-r pattern in the distance range out to about 2 Å. The data show evidence of well defined correlations in the cloudy samples out to distances of at least 11 Å, dependent on the sample. The higher-r distances are dominated by U–U correlations and are not impacted by small errors in background subtraction. The distances attributed to uranium correlations are summarized in

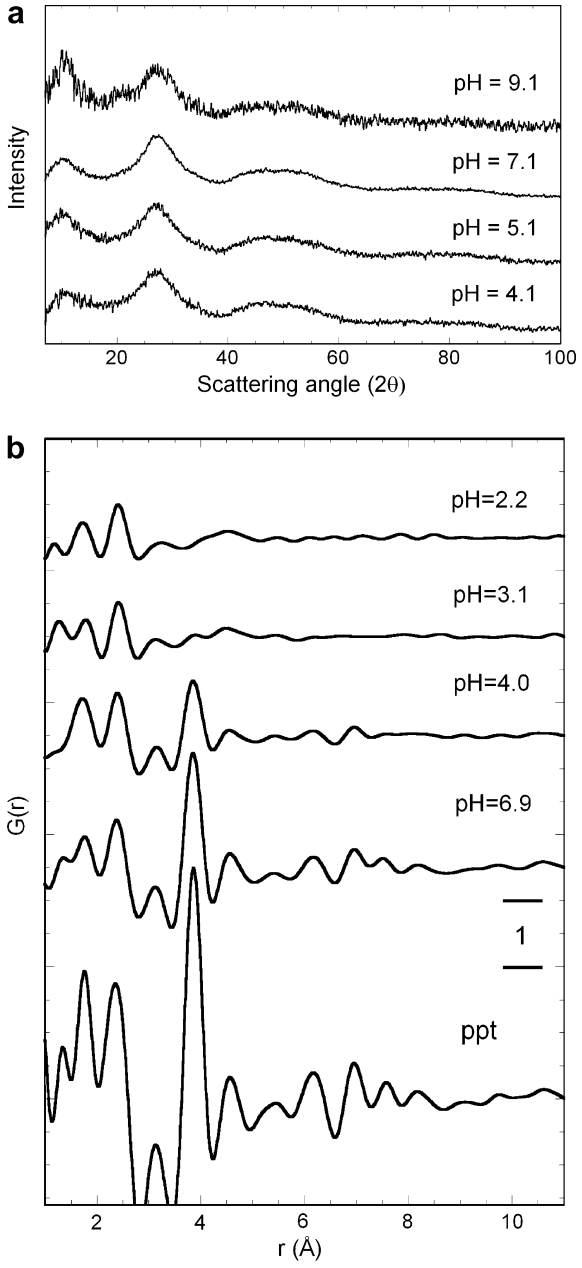

Fig. 1. (a) Exemplary XRD powder patterns obtained from centrifuged suspensions formed in the room temperature uranyl silicate solutions. The broadly oscillating intensities, combined with the absence of any Bragg peaks, is consistent with amorphous precipitates. (b) FT of HEXS data obtained on solutions or suspensions of room temperature uranyl silicate samples as a function of pH. The bottom pattern is representative of the dried precipitates that were used to obtain the XRD patterns shown in (a).

Table 1, with selected examples of correlations diagrammed in Table 2.

As seen in Fig. 1b, there is a change in the extent of the correlations as a function of pH but the distances at which the peaks are observed show little change. The FT obtained from the sample with the lowest pH of those measured, 2.2, showed no evidence for the formation of U dimers or higher oligomers, the presence of which is signified by the peak at about 4 Å that appears in the PDFs from the higher pH samples. The correlations at 1.74 and 2.42 Å, correspond to the well known coordination environment seen for U(VI) in aqueous solution (Neuefeind et al., 2004; Antonio and Soderholm, 2006) and represent the dioxo and equatorial coordination, respectively. The dioxo peak is compromised by Si–O and Cl–O correlations that have not been adequately removed. The equatorial bond distances seen in U(VI) dioxo species correlate with coordination number (Burns, 2005); the distance and intensity observed here are consistent with five coordinating oxygens in the first coordination sphere. In addition to the strong features in the data representing the first coordination shell, there are also weaker features at 3.24, 4.1, and 4.5 Å.

Whereas the FT of the HEXS data obtained from the pH 3.1 sample indicates that the U(VI) first coordination shell is indistinguishable from that seen at lower pH, there are clear changes to the PDF at longer r. The peak seen at 3.24 Å at pH 2.2 is shifted to 3.15 Å and can be attributed to a uranyl-silicate mononuclear, bidentate U–Si interaction (ICSD, 2006) as depicted in Table 2. There is also a small peak at about 3.85 Å that is consistent with a U–Si correlation from monodentate–silicate coordination and/or a U–U interaction. Although these two interactions cannot be distinguished in the HEXS data because of the experimental resolution, the data trends with increasing pH show the development of dominating U–U correlations at this distance.

The PDF obtained from the pH 4 sample shows the progression of uranyl oligomerization. The peak at 3.15 Å is more clearly defined as is the peak at 3.85 Å, which is more clearly distinguished as resulting from U–U interactions. The pronounced peak at about 4.5 Å has been previously observed in HEXS data obtained from aqueous uranyl samples, where it has been attributed to waters in the second coordination sphere (Neuefeind et al., 2004; Soderholm et al., 2005; Gutowski and Dixon, 2006). Although the intensity of the peak suggests that a more likely origin in these samples is a U–U interaction, such a correlation is not prevalent in known uranyl silicate structures (ICSD, 2006) although it is observed in metaschoepite, a uranyl oxyhydroxide (Weller et al., 2000).

At pH 5 and above, the PDF patterns, as represented by that for the pH 6.9 sample, show well defined correlations to $r = 7.5$ Å and longer, consistent with characteristic U–U correlations at those distances previously determined in single-crystal structural analyses of representative uranyl silicates.

Table 1
Correlations observed in the FT of the HEXS data on the room temperature (RT) samples shown in Fig. 1b

Distance (Å) RT-solution	Distance (Å) RT-precipitate	Correlation[a]
1.74	1.76	**U=O$_{ax}$**
2.40–2.42	2.35	**U–O$_{eq}$**
3.12–3.15	3.12	**U**–(O$_2$)–**Si** bidentate–silicate
3.85–3.86	3.84	**U**-(O$_2$)-**U**
		U–O–**Si** monodentate–silicate
4.56–4.58	4.57	**U**–x–(**H$_2$O**) second coordination H$_2$O
5.41–5.43	5.44	**U**–O–**U** oxo-bridge
6.1	6.17	**U**–O–Si–O–**U**
6.95	6.95	**U**–O–Si–O–**U**
7.5	7.57	

The bolded atoms in the last column correspond to the correlation of interest. The interactions involved in the correlations are depicted in Table 2.

[a] See pictorial description of correlation nomenclature in Table 2.

Table 2
Pictorial description of exemplary uranyl-silicate linkages and their distance ranges in known crystalline phases

		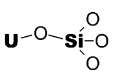	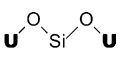
3.06 - 3.15 Å	3.84 - 3.85 Å	3.85 - 3.90 Å	5.2 - 6.4 Å
U-(O$_2$)-Si	U-(O$_2$)-U	U-O-Si	U-O-Si-O-U
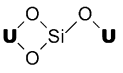	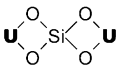	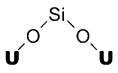	
5.82 - 5.83 Å	6.0 - 6.36 Å	6.9 - 7.1 Å	
U-O-Si-(O$_2$)-U	U-(O$_2$)-Si-(O$_2$)-U	U-O-Si-O-U	

The dioxo moieties are perpendicular to the page and not shown for clarity.

3.2. Hydrothermally treated samples

The hydrothermal samples prepared at pH 5.1–9.1 all yielded precipitates but only that from the pH 5.1 sample showed well defined narrow peaks in its XRD pattern (Fig. 2a). All of the peaks from this sample are consistent with the known structure of uranyl orthosilicate, or soddyite, $(UO_2)_2SiO_4{\cdot}(H_2O)_2$, (Demartin et al., 1992) the reported synthesis of which is similar to the conditions used to make this sample (Moll et al., 1995). The sensitivity of phase formation to solution pH is demonstrated by the XRD patterns of the precipitates obtained from the pH 6.0 to 9.1 solutions, as exemplified by the patterns obtained at pH values of 6.0, and 7.1 in Fig. 2a, and which show no evidence of crystallinity.

Exemplary HEXS data obtained from the same precipitates, shown in Fig. 2b, provide a more detailed description of the changes in uranyl speciation that occur with changes in solution pH above pH 5. Unlike the samples prepared at room temperature, the hydrothermal samples show differences in uranyl correlations, as detailed in Table 3. However, the differences occur predominately for correlations longer than about 4 Å. The peaks at distances at about

4 Å or less are attributed to U=O_{ax}, U–O_{eq}, U–O_2–Si and U–U, and remain largely invariant to changes in the pH. These peaks are also similar to those occurring in the samples synthesized at room temperature, although the peak at 3.12–3.15 Å attributed to bidentate silicate as shown in Table 2, is shifted to a slightly shorter distance, 3.06 Å. This shortening of the U–Si bidentate interaction is observed even in the sample that exhibits the powder XRD pattern that can be indexed as soddyite. The published single crystal structure of soddyite (Demartin et al., 1992) finds the same U–Si correlation at a distance of 3.157 Å, significantly longer than determined from the HEXS data. This anomaly is not understood, although it has been reported in a previous study of uranyl sorption complexes on silica (Sylwester et al., 2000). A similar distance was also observed in a study that compared known crystal structures with L_3 edge uranium EXAFS from well characterized crystalline uranyl minerals and related compounds (Catalano and Brown, 2004). Short distances were obtained from EXAFS for the bidentate U–Si correlations and attributed to interference from neighboring scattering shells. Such an explanation is not likely for the HEXS results and suggests that further work is needed to understand the origin of the peak shift.

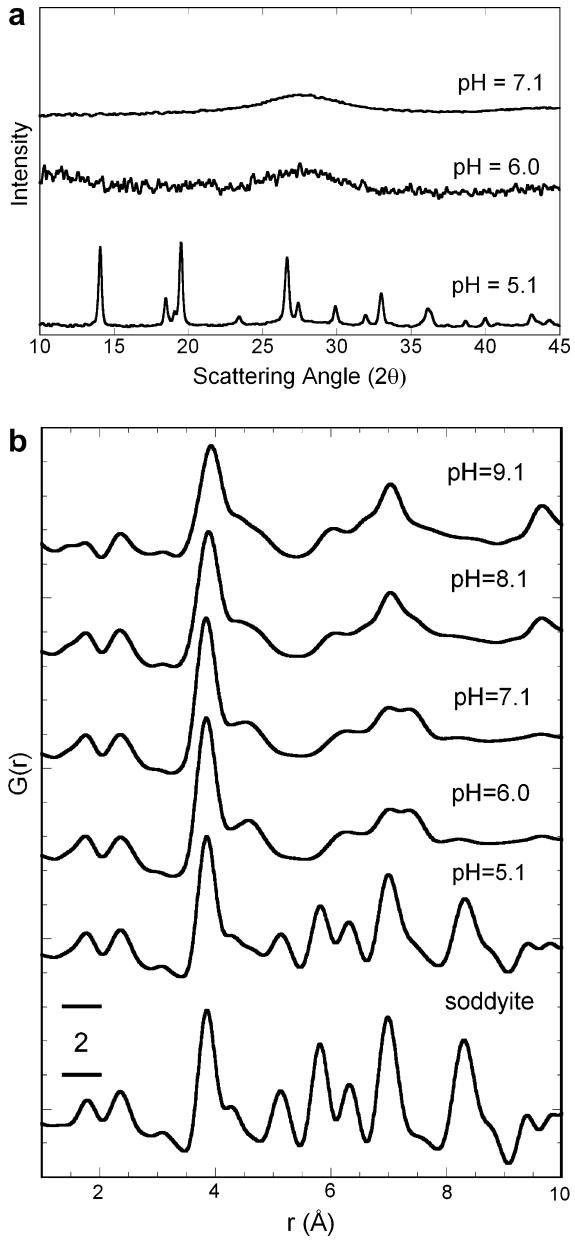

Fig. 2. (a) Exemplary XRD powder pattern obtained from precipitates formed in the hydrothermally treated uranyl silicate solutions. The diffraction pattern obtained for the pH 5.1 sample is consistent with the known pattern for soddyite. The broadly oscillating intensities found for the higher pH samples, combined with the absence of any Bragg peaks, is consistent with amorphous precipitates. (b) FT of HEXS data obtained on precipitates from hydrothermally treated uranyl silicate samples as a function of pH. Also included are the HEXS data obtained from a standard soddyite sample for direct comparison with the corresponding pattern obtained from the pH 5.1 precipitate. The pH-dependent samples are the same ones used to obtain the XRD patterns shown in Fig. 2a.

The PDF of the HEXS data from the pH 5.1 hydrothermal precipitate, which has a diffraction pattern consistent with soddyite, is compared with similarly treated HEXS data obtained from a standard soddyite sample in Fig. 2b, which was prepared as described previously (Nguyen et al., 1992). The peak positions and relative intensities both match well out to distances of 10 Å. There is a slight difference in the data in the $r = 4.1$–4.8 Å range indicating the presence of more complex correlations in the hydrothermal sample than seen in the standard.

The PDF from the pH 6.0 sample is significantly different from the soddyite standard synthesized at pH 5.1. This slightly higher pH sample exhibits fewer and broader longer-range correlations, consistent with the absence of crystallinity as determined by X-ray diffraction. The ratio of intensities of the 2.4 and 4 Å peaks is consistent with the latter correlation arising from two U–U interactions. The peak centered at 4.3 Å in the soddyite spectrum, which represents several U–O distances in the solid, (Demartin et al., 1992) is diminished and replaced by a peak at 4.58 Å. A peak at the same distance has been observed previously in thorium, (Skanthakumar and Soderholm, 2006) uranyl (Aberg et al., 1983; Neuefeind et al., 2004) and neptunyl (Soderholm et al., 2006) solutions, where it has been attributed to water coordination from the second coordination sphere. However, its higher intensity in these samples indicates that in this case the peak is more likely to originate from a single U–U interaction. The peak is significantly broadened, by a factor of three, relative to the U–U correlation at 3.9 Å, revealing that the latter interaction is significantly more rigid and hence has a smaller Debye–Waller factor or is much less disordered.

The PDF obtained from the pH 7.1 sample is both quantitatively and qualitatively similar to that from the pH 6.0 sample. In contrast, the spectrum from the pH 8.1 sample exhibits a change in correlations that persists in the pH 9.1 sample. The further change is seen for correlations in the $r = 4.1$–4.8 Å range, which appear to combine the correlations seen in the soddyite sample and the peak attributed to second coordination sphere water. In addition,

Table 3
Correlations observed in the FT of the HEXS data on solids from the hydrothermally treated solutions shown in Fig. 2b

Soddyite, Demartin et al. (1992)	Boltwoodite, Burns (1998)	pH = 5.1	pH = 6.1 and 7.0	pH = 8.1 and 9.1	
1.78	1.80	1.76	1.76	1.76	**U=O**
2.31	2.268, 2.312	2.35	2.35	2.35	**U–O_{eq}**
3.157	3.152	3.06	3.06	3.06	**U–(O_2)–Si**
3.80	3.788	3.85	3.85	3.85–3.90	**U–O–Si**
3.86	3.952				**U–O–U**
4.19, 4.21, 4.32, 4.33		4.27			**U–O–Si-O**
			4.58	4.58	**U**–x–(H_2**O**)
5.15		5.13			**U–O–Si–O–U**
5.83		5.82			**U–O–Si–(O_2)-U**
6.31, 6.36	6.05	6.30	6.26	6.04	**U–(O_2)-Si-(O_2)–U**
6.98	7.060, 7.077	7.0	7.02	7.02	**U–O–Si–O–U**
			7.36		
8.29, 8.33	8.216, 8.364	8.32	8.21		
9.41		9.42			
9.84	9.697	9.80	9.68	9.68	

The bolded letters correspond to interactions depicted graphically in Table 2.

there is a U–U longer-range correlation, at about 9.7 Å, indicating the presence of larger oligomers. Despite this observation, the X-ray diffraction pattern shows no evidence of crystallinity.

3.3. Thermodynamic modeling

Uranyl speciation can be complex even in the absence of silicates due to the formation of a wide variety of polymeric uranyl hydroxides and uranyl carbonates in solution and to precipitation of uranium bearing phases. Complicating the uranyl speciation predicted by thermodynamic models for our systems is the speciation of silica itself. The reported solubility of amorphous silica ranges from about 2 to 4 mM ($10^{-2.38}$ to $10^{-2.74}$), (Morey et al., 1964; Walther and Helgeson, 1977; Iler, 1979) significantly less than the concentrations used in the experiments discussed herein. The kinetics of amorphous silica precipitation are also quite variable. It has been reported that approximately 300 days are required to reach equilibrium from a solution supersaturated with silica, (Morey et al., 1964) however the presence of metal ions can greatly accelerate the condensation of silicate aggregates (Iler, 1979; Crerar et al., 1981; Mayo et al., 2000; Teo and Zeng, 2001; Watton et al., 2003) with ill-defined coordination properties. This is particularly noteworthy for our experimental conditions due to the necessary presence of metal ions and a silica concentration well above the amorphous solubility limit.

Uranyl speciation in our systems was modeled as a function of acidity and total silicate concentration. Table 4 lists the reactions included in our thermodynamic model together with the (zero ionic strength) equilibrium constants used in the calculations. These reactions were chosen to account for uranyl speciation in solution and the most likely thermodynamically stable solid-phases. Calculations were made using the program MEDUSA, (Puigdomenech, 2004) with activity coefficients calculated by the program for an ionic strength of 0.2 M.

Fig. 3a illustrates the uranyl speciation calculated for a fully equilibrated, closed system that contains 0.10 M silicate, the total concentration of silicate present in each of our samples. The uranyl speciation calculated using this set of parameters does not indicate the presence of significant concentrations of aqueous uranyl-silicate species. At equilibrium, the speciation is dominated by free UO_2^{2+} and soluble dinuclear uranyl hydroxides at the lowest pHs. Between pH 3 and 5, the model predicts the ingrowth of the uranyl silicate mineral soddyite at the expense of the dissolved species. Finally, over a small pH range at approximately pH 5, the stable solid phase changes from soddyite to sodium boltwoodite, $Na(H_3O)UO_2SiO_4{\cdot}H_2O$. Under these solution conditions, amorphous silica is a major silicate species at all pH values when the system is at equilibrium, as expected from reported solubility measurements (Morey et al., 1964; Walther and Helgeson, 1977).

Comparison of these modeling results with our experimental measurements suggests that using the formal silicate concentration in the thermodynamic model overestimates the silicate concentration that is available to form complexes with uranyl ions in the solutions studied herein. Silicate ions in supersaturated solutions are known to form metastable polymers, which significantly changes the speciation and solution reactivity of the polymerized ions relative to the monomers (Iler, 1979), thereby reducing the effective concentration of silicate. The formation of metastable silicate clusters is not represented within thermodynamic modeling. To better understand the behavior of the silicate species, the speciation was also modeled for sets of solutions under similar conditions (0.05 M UO_2^{2+}, 0.0003 M CO_3^{2-}, 0.2 M Na^+pH 2–10) where the total silicate concentration was varied between 0 and 0.1 M. The calculated uranyl speciation best reflects the speciation derived from the HEXS data when the formal silicate concentration is between 0.03 and 0.04 M. The computed speciation for 0.03 M formal silicate concentration is shown as a function of pH in Fig. 3b. With 0.03 M total silicate, the model predicts that the mineral soddyite is stable between pH 3.5 and 6. This solid phase, identified by XRD, was produced in our experiments from a hydrothermally treated pH 5.1 solution. In addition, the thermodynamic model for the adjusted solution composition suggests the higher pH samples will include schoepite, the phase consis-

Table 4
Equations and equilibrium constants used in thermodynamic modeling of uranyl-silicate solutions

	Log K ($I = 0$)	Reference
$UO_2^{2+} + H_2O = UO_2OH^+ + H^+$	−5.25	Guillaumont et al. (2003)
$UO_2^{2+} + 2H_2O = UO_2(OH)_2 + 2H^+$	−12.15	Guillaumont et al. (2003)
$UO_2^{2+} + 3H_2O = UO_2(OH)_3^- + 3H^+$	−20.25	Guillaumont et al. (2003)
$UO_2^{2+} + 4H_2O = UO_2(OH)_4^{2-} + 4H^+$	−32.40	Guillaumont et al. (2003)
$2UO_2^{2+} + H_2O = (UO_2)_2OH^{3+} + H^+$	−2.70	Guillaumont et al. (2003)
$2UO_2^{2+} + 2H_2O = (UO_2)_2(OH)_2^{2+} + 2H^+$	−5.62	Guillaumont et al. (2003)
$3UO_2^{2+} + 5H_2O = (UO_2)_3(OH)_5^+ + 5H^+$	−15.55	Guillaumont et al. (2003)
$3UO_2^{2+} + 7H_2O = (UO_2)_3(OH)_7^- + 7H^+$	−32.20	Guillaumont et al. (2003)
$4UO_2^{2+} + 7H_2O = (UO_2)_4(OH)_7^+ + 7H^+$	−21.90	Guillaumont et al. (2003)
$UO_2^{2+} + CO_3^{2-} = UO_2CO_3$	9.94	Guillaumont et al. (2003)
$UO_2^{2+} + 2CO_3^{2-} = UO_2(CO_3)_2^{2-}$	16.61	Guillaumont et al. (2003)
$UO_2^{2+} + 3CO_3^{2-} = UO_2CO_3{}_3^{4-}$	21.84	Guillaumont et al. (2003)
$3UO_2^{2+} + 6CO_3^{2-} = (UO_2)_3CO_3{}_6^{6-}$	54.00	Guillaumont et al. (2003)
$2UO_2^{2+} + CO_3^{2-} + 3H_2O = (UO_2)_2CO_3(OH)_3^- + 3H^+$	−0.86	Guillaumont et al. (2003)
$3UO_2^{2+} + CO_3^{2-} + 3H_2O = (UO_2)_3O(OH)_2(HCO_3)^+ + 3H^+$	0.65	Guillaumont et al. (2003)
$11UO_2^{2+} + 6CO_3^{2-} + 12H_2O = (UO_2)_{11}(CO_3)_6(OH)_{12}^{2-} + 12H^+$	36.40	Guillaumont et al. (2003)
$UO_2^{2+} + H_4SiO_4 = UO_2H_3SiO_4^+ + H^+$	−1.84	Guillaumont et al. (2003)
$H_4SiO_4 = 2H^+ + H_2SiO_4^{2-}$	−23.14	Guillaumont et al. (2003)
$H_4SiO_4 = H^+ + H_3SiO_4^-$	−9.81	Guillaumont et al. (2003)
$Na^+ + CO_3^{2-} = NaCO_3^-$	1.27	Martell (2001)
$Na^+ + CO_3^{2-} + H^+ = NaHCO_4$	10.03	Martell (2001)
$Na[UO_2(SiO_3OH)](H_2O)_{1.5} + 3H^+ = UO_2^{2+} + Na^+ + H_4SiO_4 + 1.5H_2O$	5.85	Nguyen et al. (1992)
$(UO_2)_2SiO_4(H_2O)_2 + 4H^+ = 2UO_2^{2+} + SiO_2 + 4H_2O$	6.43	Gorman-Lewis et al. (2006)
$Na_2(UO_2)_2(Si_2O_5)_3(H_2O)_4 + 6H^+ = 2UO_2^{2+} + 2Na^+ + 6SiO_2 + 7H_2O$	1.50	Nguyen et al. (1992)
$UO_2CO_3(s) = UO_2^{2+} + CO_3^{2-}$	−14.76	Guillaumont et al. (2003)
$UO_2(OH)_2(H_2O)(s) + 2H^+ = UO_2^{2+} + 3H_2O$	6.00	Martell (2001)
$Na_4UO_2(CO_3)_3(s) = 4Na^+ + UO_2^{2+} + 3CO_3^{2-}$	−27.18	Guillaumont et al. (2003)
SiO_2 (am) $+ 2H_2O = H_4SiO_4$	−2.71	Martell (2001)

tent with the PDF peak at 4.58 Å, and sodium boltwoodite. Although there are minor discrepancies in detail, the overall trends and observed tendencies to particular phase compositions are reproduced in these calculations. Observed differences in calculated and experimentally determined phases may result, at least in part, from insufficient time in our solution treatment to allow the establishment of a thermodynamic equilibrium; known procedures for the production of single-phase precipitates employ longer soaking times and slightly different solution conditions (Nguyen et al., 1992). The literature also suggests that formation of boltwoodite requires a more precise composition of the starting solution whereas soddyite can be formed from a range of initial solution compositions.

4. DISCUSSION

Taken together, the XRD, HEXS and thermodynamic modeling present a coherent picture of uranyl speciation in silicate solutions as a function of pH and provide insight into uranyl oligomerization, and the competition between related amorphous and crystalline phases.

In solutions with higher acidity, that is pH values less than about 3.5, uranyl exhibits bidentate, and possibly minor amounts of monodentate silicate coordination. This coordination is modified at slightly higher pH by the presence of well defined U–U correlations at about 3.85 Å. U–U oligomerization is also evidenced by ingrowth of longer-distance correlations that can, with the exception of a peak seen at 4.58 Å in most samples, be attributed to silicate bridged U–U interactions, most of which are exemplified in various known crystalline phases. The absence of a direct correspondence of the PDF pattern with a single known uranyl silicate phase is supported by the XRD patterns, which show no evidence of crystallinity for any of the dried precipitates obtained from the room temperature preparations.

The samples prepared at room temperature at pH 5–9 exhibit a persistent set of peaks that appear invariant to pH. The PDFs show no significant change in going from solution suspensions to centrifuged precipitates. Changes in the hydrothermal samples as a function of pH over the same pH range, together with the changing stability regions predicted by thermodynamic modeling, indicate that kinetics may play an important role in driving product formation for these samples. Changes in correlations upon aging at low temperature may be expected to result in products more similar to those seen from the hydrothermal preparations. This expectation is consistent with literature reports of changing silica speciation with time (Alexander, 1954; Tartutani, 1970 Garzó et al., 1978; Shimada and Tartutani, 1979; Iwasaki et al., 1980; Crerar et al., 1981; Shimono et al., 1983; Fitzgerald et al., 1989; Rao and Gelb, 2004; Conrad et al., 2007).

The PDFs observed for the hydrothermal samples show significant changes in uranyl correlations with pH, particularly at distance longer than about 4 Å. The observation of crystallinity in the pH 5.1 precipitate and the correspondence of its XRD pattern with that of soddyite allows for the direct assignment of longer distance correlations in

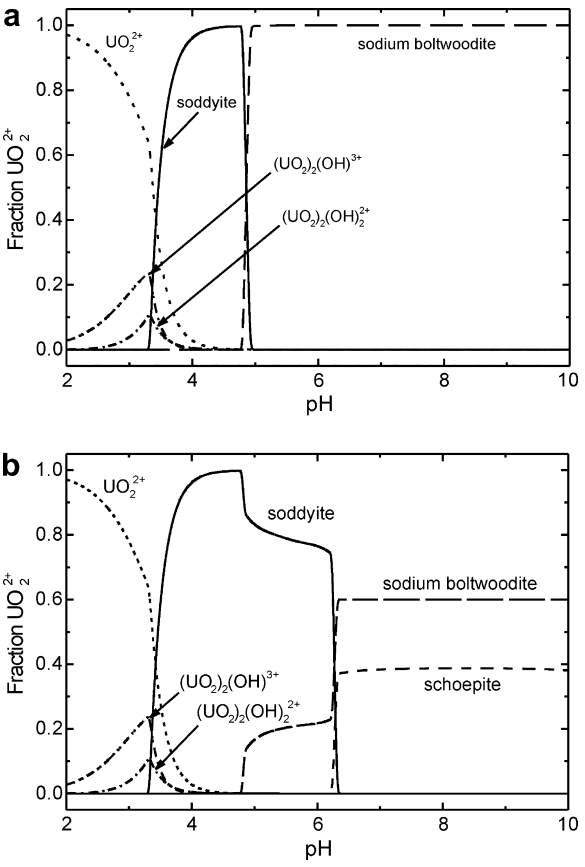

Fig. 3. (a) Fractional distribution of uranium species for a closed system containing total concentrations of 0.05 M UO_2^{2+}, 0.10 M H_4SiO_4, 0.0003 M total carbonate, and 0.2 M $NaClO_4$ at 25 °C. (b) Fractional distribution of uranium species for a closed system containing total concentrations of 0.05 M UO_2^{2+}, 0.03 M H_4SiO_4, 0.0003 M total carbonate, and 0.2 M $NaClO_4$ at 25 °C.

the PDF from the same sample. The abrupt loss of long range order for the pH 6 and higher samples is accompanied by the presence of a well defined new peak in the PDF that occurs at 4.58 Å. This peak, which is also present in the samples prepared at room temperature, is present in all of the higher pH data. Although it does not closely correspond to U–U correlations seen in crystalline silicate phases, similar distances, attributed to U–O–U interactions are observed in the uranyl oxyhydroxides schoepite (Finch et al., 1996) and metaschoepite (Weller et al., 2000). Other than this peak, the higher pH samples exhibit long-range correlations similar to those observed in boltwoodite (Burns, 1998). Notable from Table 3 is the shift in the peak seen at 6.30 Å in the PDF from the pH 5.1 sample and consistent with soddyite, to 6.04 Å in the pH 8.1 and 9.1 samples, where it is consistent with boltwoodite correlations.

In summary, the general correlations in the solutions match well with those predicted by thermodynamic modeling as depicted in Fig. 3b. At low pH uranyl coordination is dominated by monomers. Increasing pH results in a phase space dominated by soddyite. At pH above 5, schoepite becomes stable and competes with boltwoodite-like correlations about the uranyl ion. This competition of different phases prohibits the precipitation of a single phase, as evidenced by the absence of Bragg reflections in the XRD patterns obtained from samples prepared hydrothermally at pH greater than 5.1.

Interesting to note is the close similarity of all of the PDF spectra at distances out to about 4 Å. The similarity of uranyl coordination in a variety of silicates has been observed before, where it has inhibited attempts to use EXAFS as a tool to distinguish uranyl mineral phases (Thompson et al., 1997; Catalano and Brown, 2004; Catalano et al., 2004). Seen within this broader picture that includes longer distance correlations, it points to a perspective that can be used to understand uranyl silicate chemistry. The PDF correlations and their intensities can be accounted for by assuming the stability of a fundamental uranyl-silicate coordination, such as shown in Fig. 4, which includes five coordinating oxygens at a distance of about 2.4 Å. The oxygens originate from one bidentate silicate, and four silicates bridging two uranyl ions. This species can be considered as a building block, or synthon, that is preorganized and present in all the solutions in our study that contain oligomeric uranyl silicates. The correlations occurring in the synthon shown in Fig. 4 are compared with a standard PDF derived from experiment in Fig. 5. The observed longer range correlations can be viewed as organization or correlations that arise from the aggregation of these synthons. Within this context, which one of the larger aggregates forms depends on two different competitive bonding paths. The first involves a competition for the –OR site shown in Fig. 4. In soddyite, this position is occupied by a H_2O ligand, (Demartin et al., 1992) whereas in the uranophane group with U:Si = 1:1, which includes boltwoodite (Burns, 1998) or in sodium weeksite, $Na_2(UO_2)_2$·

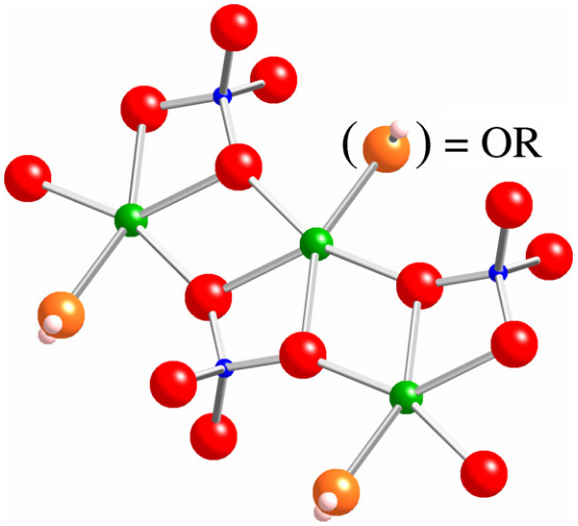

Fig. 4. The proposed synthon that serves as a building block for the uranyl silicate structures observed in the HEXS data as correlations. U (green), Si (blue), O (red), and H_2O (orange/pink) form the basic unit. The oxo links to uranyl, which are oriented perpendicular to the page, have been omitted for clarity. The –OR moiety (orange), depicted here as water can be substituted by silicate to change the observed correlations from those found in soddyite to structures seen in boltwoodite and weeksite. (For interpretation of the references to color in this figure legend, the reader is referred to the web version of this paper.)

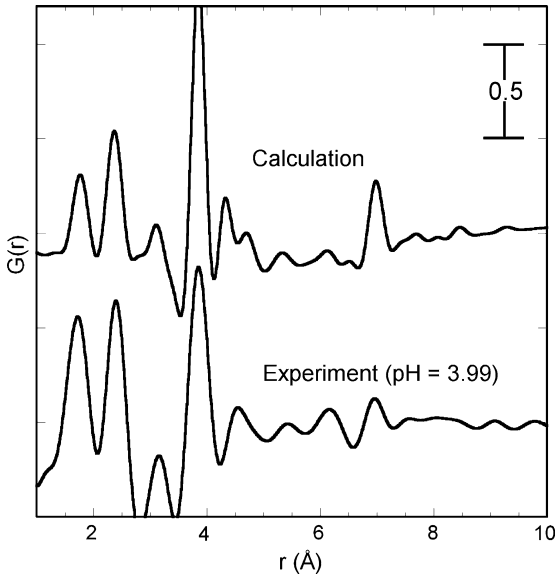

Fig. 5. A comparison of the correlations expected from the synthon depicted in Fig. 4 (and including the dioxo ligation to U^{6+}) with those observed from experiment. The correlation observed at about 7 Å corresponds to the longer, U–U trimer correlation.

$(Si_2O_5)_3{\cdot}4H_2O$ with U:Si = 2:5 (Jackson and Burns, 2001) the water is replaced by an orthosilicate group. The binding of this silicate group to other uranyl ions or interstitial cations is what distinguishes the different phases. The second competitive path is associated with the deprotonation of silicate-oxygens associated with the synthon. Viewed from this perspective, the synthesis of single-phase crystalline uranyl silicate samples requires conditions that favor the predominance of one form of synthon linkage. In the experiments described herein, those conditions occurred when the –OR ligation was water and the bound silicates were deprotonated. Evidence for the replacement of water by an oxo-bridged uranyl group at pHs greater than 5.1 is seen by the occurrence of the peak 4.58 Å in the PDFs of all the amorphous samples. A mechanistic pathway is suggested for the transition from soddyite to boltwoodite predicted from the thermodynamic modeling to occur near pH 5 under the chemical conditions of this study. Until the concentration of protons in solution is low enough to allow aqueous silicate to compete for the core uranyl synthon, soddyite persists. Once the pH is high enough, the coordinated water is replaced to yield the synthon of boltwoodite. The concept of building three dimensional structures from dissolved synthons has been recently proposed based on HEXS data of a dissolved Th dimer (Wilson et al., 2007).

5. CONCLUSIONS

Except for solutions at low pH, all samples showed evidence of significant uranyl oligomerization. HEXS data show evidence of correlations out to distances of 10 Å or longer in selected cases despite the absence of long range order as judged by the absence of peaks in the XRD patterns. The similarity in correlations obtained from all the higher pH samples prepared at room temperature indicates a kinetic control on product formation. In contrast, the hydrothermal samples showed considerable variety in U–U correlations that point to an evolution from soddyite, which is seen as a crystalline phase at pH 5.1, through a mixed phase that includes schoepite- and boltwoodite-like correlations to pH 9.1. These results are supported by thermodynamic modeling of phase stabilities under conditions relevant to the solutions. Strong similarities in all HEXS spectra, from samples with pHs greater than 3.1, in correlations at distances out to 4 Å suggest a model in which a building block, or synthon, is preorganized in solution. Changes in mid-range correlations as a function of pH are the result of changes in how the synthons themselves organize and not on fundamental changes in uranyl coordination. Structural motifs corresponding to mineral phases are then built up by linking of the pre-existing synthons. Attempts to classify or associate amorphous samples as known mineral phases imply well defined crystalline structures. Redefining these amorphous systems in terms of synthons and their relative occurrence provides a more flexible framework in which to discuss these systems. Crystallinity can then be thought of as an outgrowth of solution species that occurs when selected synthon linkages result in long range order.

ACKNOWLEDGMENTS

The authors wish to thank Jeffrey G. Catalano for helpful discussions. This work was funded by the U.S. Department of Energy, Office of Biological and Environmental Research, Environmental Remediation Sciences Program under grant number DE-FG02-06ER64193 to the University of Illinois at Chicago and Contract DE-AC02-06CH11357 to Argonne National Laboratory. The HEXS data were measured at beamline 11-ID-B of the Basic Energy Sciences Synchrotron Radiation Center (BESSRC), Advanced Photon Source (APS). Use of the Advanced Photon Source was supported by the U.S. Department of Energy, Office of Science, Office of Basic Energy Sciences, also under Contract No. DE-AC02-06CH11357.

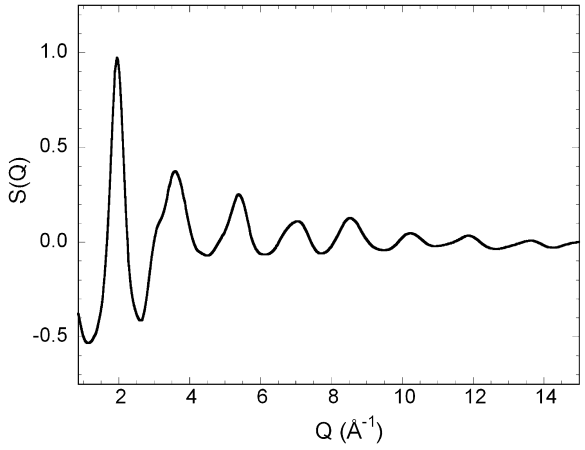

Fig. A1. A representative HEXS scattering function (Skanthakumar and Soderholm, 2006) obtained from the hydrothermally treated pH 6.0 sample. The FT of this function is displayed in Fig. 2b. The XRD pattern from the same sample is shown in Fig. 2a.

APPENDIX A

See Fig. A1.

REFERENCES

Aberg M., Ferri D., Glaser J. and Grenthe I. (1983) Structure of the hydrated dioxouranium (VI) ion in aqueous solution. An X-ray diffraction and ^{1}H NMR study. *Inorg. Chem.* **22**, 3986–3989.

Alexander G. B. (1954) The polymerization of monosilicic acid. *J. Am. Chem. Soc.* **76**, 2094–2096.

Allard T., Ildefonse P., Beaucaire C. and Calas G. (1999) Structural chemistry of uranium associated with Si, Al, Fe gels in a granitic uranium mine. *Chem. Geol.* **158**, 81–103.

Antonio M. R. and Soderholm L. (2006) X-ray absorption spectroscopy of the actinides. In *Chemistry of the Actinide and Transactinide Elements* (eds. L. R. Morss, J. Fuger and N. Edelstein). Springer, Dordrecht.

Arai Y., McBeath M., Bargar J. R., Joye J. and Davis J. A. (2006) Uranyl adsorption and surface speciation at the imogolite-water interface: self-consistent spectroscopic and surface complexation models. *Geochim. Cosmochim. Acta* **70**, 2492–2509.

Burns P. C. (1998) The structure of boltwoodite and implications of solid solution toward sodium boltwoodite. *Can. Mineral.* **36**, 1069–1075.

Burns P. C. (2005) U^{6+} minerals and inorganic compounds: insights into an expanded structural hierarchy of crystal structures. *Can. Mineral.* **43**, 1839–1894.

Catalano J. G. and Brown G. E. J. (2004) Analysis of uranyl-bearing phases by EXAFS spectroscopy: interferences, multiple scattering, accuracy of structural parameters, and spectral differences. *Am. Mineral.* **89**, 1004–1021.

Catalano J. G., Heald S. M., Zachara J. M. and Brown G. E. J. (2004) Spectroscopic and diffraction study of uranium speciation in contaminated vadose zone sediments from the Handford site, Washington State. *Environ. Sci. Technol.* **38**, 2822–2828.

Chisholm-Brause C., Conradson S. D., Buscher C. T., Eller P. G. and Morris D. E. (1994) Speciation of uranyl sorbed at multiple-binding sites on montmorillonite. *Geochim. Cosmochim. Acta* **58**, 3625–3631.

Cho H., Felmy A. R., Craciun R., Keenum J. P., Shah N. and Dixon D. A. (2006) Solution state structure determination of silicate oligomers by Si-29 NMR spectroscopy and molecular modeling. *J. Am. Chem. Soc.* **128**, 2324–2335.

Conrad C. F., Icopini G. A., Yasuhara H., Bandstra J. Z., Brantley S. L. and Heaney P. J. (2007) Modeling the kinetics of silica nanocolloid formation and precipitation in geologically relevant aqueous solutions. *Geochim. Cosmochim. Acta* **71**, 531–542.

Crerar D. A., Axtmann E. V. and Axtmann R. C. (1981) Growth and ripening of silica polymers in aqueous solutions. *Geochim. Cosmochim. Acta* **45**, 1259–1266.

Demartin F., Gramaccioli C. M. and Pilati T. (1992) The importance of accurate crystal structure determination of uranium minerals. II. Soddyite $(UO_2)_2SiO_4(H_2O)_2$. *Acta Crystallogr. C* **48**, 1–4.

Dent A. J., Ramsay J. D. F. and Swanton S. W. (1992) An EXAFS study of uranyl ion in solution and sorbed onto silica and montmorillonite clay colloids. *J. Colloid Interface Sci.* **150**, 45–60.

Egami T. and Billinge S. J. L. (2003) *Underneath the Bragg Peaks: Structural Analysis of Complex Materials*. Pergamon, Amsterdam.

Finch R. and Murakami T. (1999) Systematics and paragenesis of uranium minerals. In *Uranium: Mineralogy, Geochemistry, and the Environment* (eds. P. C. Burns and R. Finch). Mineralogical Society of America, Washington, DC.

Finch R. J., Cooper M. A., Hawthorne F. C. and Ewing R. C. (1996) The crystal structure of schoepite, $(UO_2)_8O_2(OH)_{12}(H_2O)_{12}$. *Can. Mineral.* **34**, 1071–1088.

Fitzgerald J. J., Hoffman J. A. and Nebo C. O. (1989) Applications of gel filtration chromatography to the study of aqueous silicate complexes. *J. Chromatogr. Sci.* **27**, 186–192.

Froideval A., Del Nero M., Barillon R., Hommet J. and Mignot G. (2003) pH dependence of uranyl retention in a quartz/solution system: an XPS study. *J. Colloid Interface Sci.* **266**, 221–235.

Frost R. L., Cejka J., Weier M. L. and Martens W. (2006a) Molecular structure of the uranyl silicates—a Raman spectroscopic study. *J. Raman. Spectrosc.* **37**, 538–551.

Frost R. L., Cejka J., Weier M. L., Martens W. and Kloprogge J. T. (2006b) A Raman and infrared spectroscopic study of the uranyl silicates-Weeksite, soddyite, and haiweeite. *Spectrochim. Acta* **A64**, 308–315.

Gabriel U., Charlet L., Schläpfer C. W., Vial J. C., Brachmann A. and Geipel G. (2001) Uranyl surface speciation on silica particles studied by time-resolved laser-induced fluorescence spectroscopy. *J. Colloid Interface Sci.* **239**, 358–368.

Garzó G., Hoebbel D., Ecsery Z. J. and Ujszászi K. (1978) Gas chromatography of trimethylsilylated silicate anions. Separation with glass capillary columns and new aspects in derivatization. *J. Chromatogr.* **167**, 321–336.

Giaquinta D. M., Soderholm L., Yuchs S. E. and Wasserman S. R. (1997) The speciation of uranium in a smectite clay: evidence for catalysed uranyl reduction. *Radiochim. Acta* **76**, 113–121.

Gorman-Lewis D., Mazeina L., Fein J. B., Szymanowski J., Burns P. C. and Navrotsky A. (2006) Thermodynamic properties of soddyite from solubility and calorimetric measurements. *J. Chem. Thermodyn.* **39**, 568–575.

Guillaumont R., Fanghanel T., Fuger J., Grenthe I., Neck V., Palmer D. and Rand M. (2003) *Update on the Chemical Thermodynamics of Uranium, Neptunium, and Plutonium*. Elsevier, Amsterdam.

Gutowski K. E. and Dixon D. A. (2006) Predicting the energy of the water exchange reaction and free energy of solvation for the uranyl ion in aqueous solution. *J. Phys. Chem. A* **110**, 8840–8856.

Harris R. K., Knight C. T. G. and Smith D. N. (1980) Polymerization of the silicate anion in acidic solutions: silicon-29 NMR studies. *Chem. Commun.*, 726–728.

Harris R. K. and Newman R. H. (1977) ^{29}Si NMR studies of aqueous silicate solutions. *J. Chem. Soc. Faraday Trans. 2* **73**, 1204–1215.

Hill F. C. (1999) Identification of uranium-bearing minerals and inorganic phases by X-ray powder diffraction. In *Uranium Mineralogy, Geochemistry, and the Environment* (eds. P. C. Burns and R. Finch). Mineralogical Society of America, Washington, DC.

Hrnecek E. and Irlweck K. (1999) Formation of uranium(VI) complexes with monomeric and polymeric species of silicic acid. *Radiochim. Acta* **87**, 29–35.

Hudson E. A., Terminello L. J., Viani B. E., Denecke M. A., Reich T., Allen P. G., Bucher J. J., Shuh D. K. and Edelstein N. (1999) The structure of U^{6+} sorption complexes on vermiculite and hydrobiotite. *Clays Clay Miner.* **47**, 439–457.

ICSD (2006) Inorganic Structural Data Base. *FIZ and NIST*.

Iler R. K. (1979) *The Chemistry of Silica*. Wiley Interscience, New York.

Iwasaki H., Shimada K. and Tartutani T. (1980) Gel chromatographic study of the polymerization of silicic acid in acid solution. *J. Chromatogr.* **198**, 429–434.

Jackson J. M. and Burns P. C. (2001) A re-evaluation of the structure of weeksite, a uranyl silicate framework mineral. *Can. Mineral.* **39**, 187–195.

Jensen M. P. and Choppin G. R. (1998) Complexation of uranyl(VI) by aqueous orthosilicic acid. *Radiochim. Acta* **82**, 83–88.

Liu C., Zachara J. M., Qafoku O., McKinley J. P., Heald S. M. and Wang Z. (2004) Dissolution of uranyl microprecipitates in subsurface sediments at Hanford Site USA. *Geochim. Cosmochim. Acta* **68**, 4519–4537.

Magini M., Licheri G., Paschina G., Piccaluga G. and Pinna G. (1988) *X-ray Diffraction of Ions in Aqueous Solutions: Hydration and Complex Formation*. CRC Press Inc., Boca Raton.

Martell, A. E. (2001) NIST Critically Selected Stablity Constants of Metal Complexes, Database, 6.0 for Windows. U.S. Department of Commerce, Technology Administration, National Institute of Standards and Technology, Gaithersburg, MD.

Mayo E. I., Poore D. D. and Stiegman A. E. (2000) Catalysis of the silica sol-gel process by divalent transition metal bis(acetylacetonate) complexes. *Inorg. Chem.* **39**, 899–905.

McKinley J. P., Zachara J. M., Liu C., Heald S. M., Prenitzer B. I. and Kempshall B. W. (2006) Microscale controls on the fate of contaminant uranium in the vadose zone, Hanford Site, Washington. *Geochim. Cosmochim. Acta* **70**, 1873–1887.

Moll H., Geipel G., Brendler V., Bernhard G. and Nitsche H. (1998) Interaction of uranium(VI) with silicic acid in aqueous solutions studied by time-resolved laser-induced fluorescence spectroscopy (TRLFS). *J. Alloys Compounds* **271–273**, 765–768.

Moll H., Matz W., Schuster G., Brendler E., Bernhard G. and Nitsche H. (1995) Synthesis and characterization of uranyl orthosilicate $(UO_2)_2SiO_4{\cdot}2H_2O$. *J. Nucl. Mater.* **227**, 40–49.

Morey G. W., Fournier R. O. and Rowe J. J. (1964) The solubility of amorphous silica at 25 °C. *J. Geophys. Res.* **26**, 1029–1043.

Neuefeind J., Soderholm L. and Skanthakumar S. (2004) Experimental coordination environment of uranyl(VI) in aqueous solution. *J. Phys. Chem. A* **108**, 2733–2739.

Nguyen S. N., Silva R. J., Weed H. C. and Andrews J. E. J. (1992) Standard Gibbs free energies of formation at the temperature 303.15 K of four uranyl silicates: soddyite, uranophane, sodium boltwoodite, and sodium weeksite. *J. Chem. Thermodyn.* **24**, 359–376.

Plesko E. P., Scheetz B. E. and White W. B. (1992) Infrared vibrational characterization and synthesis of a family of hydrous alkali uranyl silicates and hydrous uranyl silicate minerals. *Am. Mineral.* **77**, 431–437.

Porter R. A. and Weber W. J. (1971) The interaction of silicic acid with iron(III) and uranyl ions in dilute aqueous solution. *J. Inorg. Chem.* **33**, 2443–2449.

Puigdomenech, I. (2004) MEDUSA. Royal Institute of Technology, Stockholm.

Rao N. Z. and Gelb L. D. (2004) Molecular dynamics simulations of the polymerization of aqueous silicic acid and analysis of the effects of concentration on silica polymorph distributions, growth mechanisms, and reaction kinetics. *J. Phys. Chem. B* **108**, 12418–12428.

Reich T., Moll H., Arnold T., Denecke M. A., Hennig C., Geipel G., Bernhard G., Nitsche H., Allen P. G., Bucher J. J., Edelstein N. M. and Shuh D. K. (1998) An EXAFS study of uranium(VI) sorption onto silica gel and ferrihydrite. *J. Electron Spectrosc. Rel. Phenom.* **96**, 237–243.

Reich T., Moll H., Denecke M. A., Geipel G., Bernhard G., Nitsche H., Allen P. G., Bucher J. J., Kaltsoyannis N., Edelstein N. and Shuh D. K. (1996) Characterization of hydrous uranyl silicate by EXAFS. *Radiochim. Acta* **74**, 219–223.

Satoh I. and Choppin G. R. (1992) Interaction of uranyl(VI) with silicic acid. *Radiochim. Acta* **56**, 85–87.

Shimada K. and Tartutani T. (1979) Gel chromatographic study of the polymerization of silicic acid. *J. Chromatogr.* **168**, 401–406.

Shimono T., Isobe T. and Tartutani T. (1983) Study of the polymerization of silicic acid in aqueous solution by trimethylsilylation-gas chromatography. *J. Chromatogr.* **258**, 73–80.

Skanthakumar S., Antonio M. R., Wilson R. E. and Soderholm L. (2007) The curium aqua ion. *Inorg. Chem.* **46**, 3485–3491.

Skanthakumar S. and Soderholm L. (2006) Studying actinide correlations in solution using high-energy x-ray scattering. *Mat. Res. Soc. Symp. Proc.* **893**, 411–416.

Soderholm L., Skanthakumar S., Burns P. C. and Forbes T. (2006) Similarities between the coordination of actinide ions in solution and the structure of their related crystalline phases. *Mat. Res. Soc. Symp. Proc.* **893**, 295–303.

Soderholm L., Skanthakumar S. and Neuefeind J. (2005) Determination of actinide speciation in solutions using high-energy X-ray scattering. *Anal. Bioanal. Chem.* **383**, 48–55.

Sylwester E. R., Hudson E. A. and Allen P. G. (2000) The structure of uranium (VI) sorption complexes on silica, alumina, and montmorillonite. *Geochim. Cosmochim. Acta* **64**, 2431–2438.

Tartutani T. (1970) Chromatographic behavior of silicic acid on sephadex columns. *J. Chromatogr.* **50**, 523–526.

Teo S. H. and Zeng H. C. (2001) Surface and textural properties of network-modified silica as a function of transition metal dopant zirconium. *J. Phys. Chem. B* **105**, 9093–9100.

Thompson H. A., Brown G. E. J. and Parks G. A. (1997) XAFS spectroscopic study of uranyl coordination in solids and aqueous solution. *Am. Mineral.* **82**, 483–496.

Waite T. D., Davis J. A., Fenton B. R. and Payne T. E. (2000) Approaches to modeling uranium(VI) adsorption on natural mineral assemblages. *Radiochim. Acta* **88**, 687–693.

Walter M., Arnold T., Geipel G., Scheinost A. and Bernhard G. (2005) An EXAFS and TRLFS investigation of uranium(VI) sorption to pristine and leached albite surfaces. *J. Colloid Interface Sci.* **282**, 293–305.

Walther J. V. and Helgeson H. C. (1977) Calculation of thermodynamic properties of aqueous silica and solubility of quartz and its polymorphs at high pressure and temperatures. *Am. J. Sci.* **277**, 1315–1351.

Wang Z., Zachara J. M., Gassman P. L., Liu C., Odeta Q., Wassana Y. and Catalano J. G. (2005) Fluorescence spectroscopy of U(VI)-contaminated Hanford sediment. *Geochim. Cosmochim. Acta* **69**, 1391–1403.

Watton, S. P., Taylor, C. M., Kloster, G. M. and Bowman, S. C. (2003) Coordination complexes in sol-gel silica materials, *Prog. Inorg. Chem.* **51**.

Weller M. T., Light M. E. and Gelbrich T. (2000) Structure of uranium (VI) oxide dihydrate UO_32H_2O; Synthetic meta-schoepite $(UO_2)_4O(OH)_6{\cdot}5H_2O$. *Acta Crystallogr.* **B56**, 577–583.

Wilson R. E., Skanthakumar S., Sigmon G., Burns P. C. and Soderholm L. (2007) Structure of dimeric hydrolysis products of thorium. *Inorg. Chem.* **46**, 2368–2372.

Yusov A. B. and Fedoseev A. M. (2005) A spectrophotometric study of the interaction of uranyl ions with orthosilicic acid and polymeric silicic acids in aqueous solutions. *Radiochemistry* **47**, 345–351.

Associate editor: David J. Wesolowski